

# Unveiling the bosons in an ultra-short single electron pulse

Gregoire Roussely<sup>†,1</sup>, Everton Arrighi<sup>†,1</sup>, Giorgos Georgiou,<sup>1,2</sup> Shintaro Takada,<sup>1,3</sup>  
Martin Schalk,<sup>1</sup> Matias Urdampilleta,<sup>1</sup> Arne Ludwig,<sup>4</sup> Andreas D. Wieck,<sup>4</sup> Pacome  
Armagnat,<sup>5</sup> Thomas Kloss,<sup>5</sup> Xavier Waintal,<sup>5</sup> Tristan Meunier,<sup>1</sup> and Christopher Bäuerle<sup>1</sup>

<sup>1</sup>Univ. Grenoble Alpes, CNRS, Grenoble INP, Institut Néel, 38000 Grenoble, France

<sup>2</sup>Univ. Savoie Mont-Blanc, CNRS, IMEP-LAHC, 73370 Le Bourget du Lac, France

<sup>3</sup>National Institute of Advanced Industrial Science and Technology (AIST),

National Metrology Institute of Japan (NMIJ), Tsukuba, Ibaraki 305-8563, Japan

<sup>4</sup>Lehrstuhl für Angewandte Festkörperphysik, Ruhr-Universität Bochum,  
Universitätsstrasse 150, 44780 Bochum, Germany.

<sup>5</sup>Univ. Grenoble Alpes, CEA, INAC-Pheliqs, 38000 Grenoble, France

**Quantum dynamics is very sensitive to dimensionality. While two-dimensional electronic systems form Fermi liquids, one-dimensional systems – Tomonaga-Luttinger liquids – are described by purely bosonic excitations, even though they are initially made of fermions [1, 2]. With the advent of coherent single electron sources [3, 4], the quantum dynamics of such a liquid is now accessible at the single electron level. Here, we report on time-of-flight measurements of ultra-short single electron charge pulses injected into a quasi one-dimensional quantum conductor. We change the confinement potential from the one-dimensional Tomonaga-Luttinger liquid limit to the multi-channel Fermi liquid. Our measurements show that the plasmon velocity can be varied over almost an order of magnitude, even in the quantum regime where the pulses carry one or less electrons. These results are in quantitative agreement with a parameter-free theory and demonstrate a powerful new probe for directly investigating real-time dynamics of fractionalisation phenomena in low-dimensional conductors.**

A fundamental difference between bosons and fermions is that the former can be described at the classical macroscopic level while the latter cannot. In particular, in an ultrafast quantum nanoelectronics setup, the experimentalist controls the - bosonic - electromagnetic degrees of the system and aims at injecting a single - fermionic - coherent electron in the system. This interplay between bosonic and fermionic statistics is a central feature in one-dimensional (1D) quantum systems as it provides a unique playground for the study of interaction effects [2].

The reduced dimensionality influences the interaction between particles and can lead to fascinating phenomena such as spin-charge separation [5], charge fractionalisation [6] or Wigner crystallisation [7]. The low energy collective bosonic excitations consist of charge and spin density waves that propagate with two different velocities. While the spin density is unaffected by Coulomb interaction and propagates at Fermi velocity  $v_F$ , the charge density is strongly renormalised by the interactions and

propagates with the plasmon velocity  $v_P$ , which is usually much faster than the Fermi velocity. Spin-charge separation has been experimentally probed in momentum resolved tunnelling experiments between two quantum wires [5] as well as tunnelling from a quantum wire into a two-dimensional electron gas [8]. In addition to spin-charge separation, charge fractionalisation occurs in one-dimensional systems [9]. Injecting an electron into a 1D system with momentum conservation, the charge decomposes into right and left moving charge excitations, as demonstrated in ref. [6]. Charge fractionalisation also occurs in a system of two coupled Tomonaga-Luttinger liquids. There, an electronic excitation present in one of the two channels fractionalises into a *fast* charge mode and a *slow* neutral mode, which are the eigenmodes of the coupled system [10]. This charge fractionalisation has been recently observed in a chiral two-channel Tomonaga-Luttinger liquid in the integer quantum Hall regime [11–14].

Here we study the most general case where the system can be tuned *continuously* from a clean one-channel Luttinger Liquid to a multi-channel Fermi liquid in a non-chiral system. We use time-resolved measurement techniques [15, 16] to determine the time-of-flight [17–19] of a single electron voltage pulse and extract the collective charge excitation velocity. Our detailed modeling of the electrostatics of the sample allows us to construct the excitations of the system in a parameter-free theory. We show that our self-consistent calculations capture remarkably well the results of the measurements, validating the construction of the bosonic collective modes from the fermionic degrees of freedom.

We tailored a 70 micrometer long quasi one-dimensional wire into a two-dimensional electron gas using metallic surface gates as shown in Fig. 1a. A pump and probe technique has been implemented to measure in a time-resolved manner the shape as well as the propagation speed of the electron pulse. We apply an ultra-short voltage pulse ( $\approx 70$  ps) to the left ohmic contact to generate the single electron pulse. The pulse injection is repeated at a frequency of 600 MHz and the resulting DC current is measured at the right ohmic con-

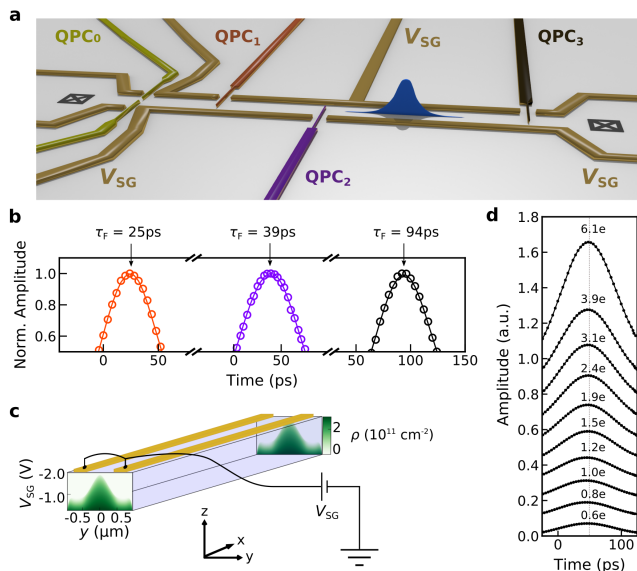


**FIG. 1: Device and time-of-flight measurements.** **a**, Schematic of the quantum device. A single electron pulse is launched at the left ohmic contact (black crossed box) by applying a very short ( $\approx 70$  ps) voltage pulse. Three QPCs, denoted as QPC<sub>1</sub>, QPC<sub>2</sub> and QPC<sub>3</sub> are placed along the quantum device at a distance of 15, 30 and 70  $\mu\text{m}$  from the left ohmic contact. Each of these three QPCs is connected to a large bandwidth (40 GHz) bias tee and operated as an ultra-fast switch. Time resolved detection of current is done at the right ohmic contact. QPC<sub>0</sub>, placed a distance of 6  $\mu\text{m}$  from the left ohmic contact is used as a channel filter. **b**, Time-resolved measurements of an electron pulse at the three different QPC positions. **c**, Illustration of the sample geometry used for the self consistent calculations. The quasi 1D quantum wire is defined by the two long electrostatic gates at potential  $V_{\text{SG}}$ . The colored images, one at the beginning of the wire and another one at the end, are cross sections of the electron density profile along the  $y$ -axis as a function of the gate voltage. **d**, Time-resolved measurements of an electron pulse at QPC<sub>3</sub> for different excitation amplitudes. The amount of electrons contained in the electron pulse is varied between 0.6e and 6.1e.

tact. Three quantum point contacts (QPCs) are placed along the quantum wire to measure the arrival time of the charge pulse at different positions. Simultaneously, another ultra-short voltage pulse is sent to one of the three QPCs which allows opening and closing the QPC on a timescale much faster than the width of the single electron pulse (see methods section). By changing the time-delay between launching the electron pulse and the on-off switching of the QPC we can reconstruct the actual shape of the single electron pulse [17, 18].

A typical time resolved measurement is shown in Fig. 1b. We observe a single electron pulse of Gaussian shape with a FWHM of  $\approx 70$  ps. Measurements of the time-of-flight  $\tau_F$  at different positions (Fig. 1b) allows us to determine its propagation speed, which we find to be independent of the number of electrons contained in the

electron pulse (Fig. 1d). By changing the voltage on the side gates  $V_{\text{SG}}$  it is possible to modify the propagation speed by almost an order of magnitude. As the confinement is made stronger, the arrival time of the electron pulse at the detection QPC is shifted to longer times, as seen in Fig. 2a. This, as it will be elucidated further on, is an indication of a slower propagation speed and it is in stark contrast to standard DC measurements. Indeed, in DC the Coulomb interaction is screened by the Fermi sea and the electrons travel at the Fermi velocity, as shown by magnetic focusing experiments [20]. The situation is very different when creating a local perturbation of the charge density. Applying a very short charge pulse results in an excess charge density created locally. Due to the generated electric field, the excess charge is displaced very rapidly at the surface of the Fermi sea giving rise to a collective excitation, a plasmon [21].

In one dimension, an interacting wire is described by Tomonaga-Luttinger plasmons of bosonic character. The problem of generalising the bosonization construction to a system containing an arbitrary number of conduction channels,  $N$ , in presence of Coulomb interactions has been treated theoretically by Matveev and Glazman [22]. The effect of the Coulomb potential is to couple the individual channels of the quantum wire, thus resulting in a collective behaviour that in turn affects strongly the propagation velocity of the excitations. For a quantum wire containing  $N$  conduction channels, Coulomb interaction leads to charge fractionalisation into  $N$  charge modes with renormalised propagation velocity and  $N$  spin modes (see suppl. material). As the spin modes do not carry any charge, their speed is not affected by the Coulomb interaction. For our experiment we can neglect them since voltage pulses do not excite spin modes in the quantum conductor. The  $N$  charge modes, on the other hand, are affected by the Coulomb interaction in the following way:  $N-1$  charge modes - the *slow* modes - are weakly affected and propagate with a speed close to  $v_F$  while one mode - the *fast* mode - usually referred to as the plasmon mode is renormalised via all the other modes and propagates with a velocity much faster than  $v_F$ . Here, we have derived the theory [22] from first principles in order to obtain a quantitative - parameter free - comparison with the measurements. Our calculations proceed in three steps: first we solve the self-consistent Electrostatics-Quantum mechanics problem to obtain the effective potential seen by the electrons as shown in Fig. 1c. Second, we compute the effective propagating channels and their interaction matrix and third we compute the plasmon velocity as arising from bosonisation theory (see suppl. material). The obtained theoretical curve, *without any adjustable parameters*, is displayed in Fig. 2b. The agreement with experiments over the entire gate voltage region is quite remarkable. We attribute the discrepancy observed in the limit of large number of channels  $N \sim 20-40$  to interchannel forward scattering which is not taken into account in

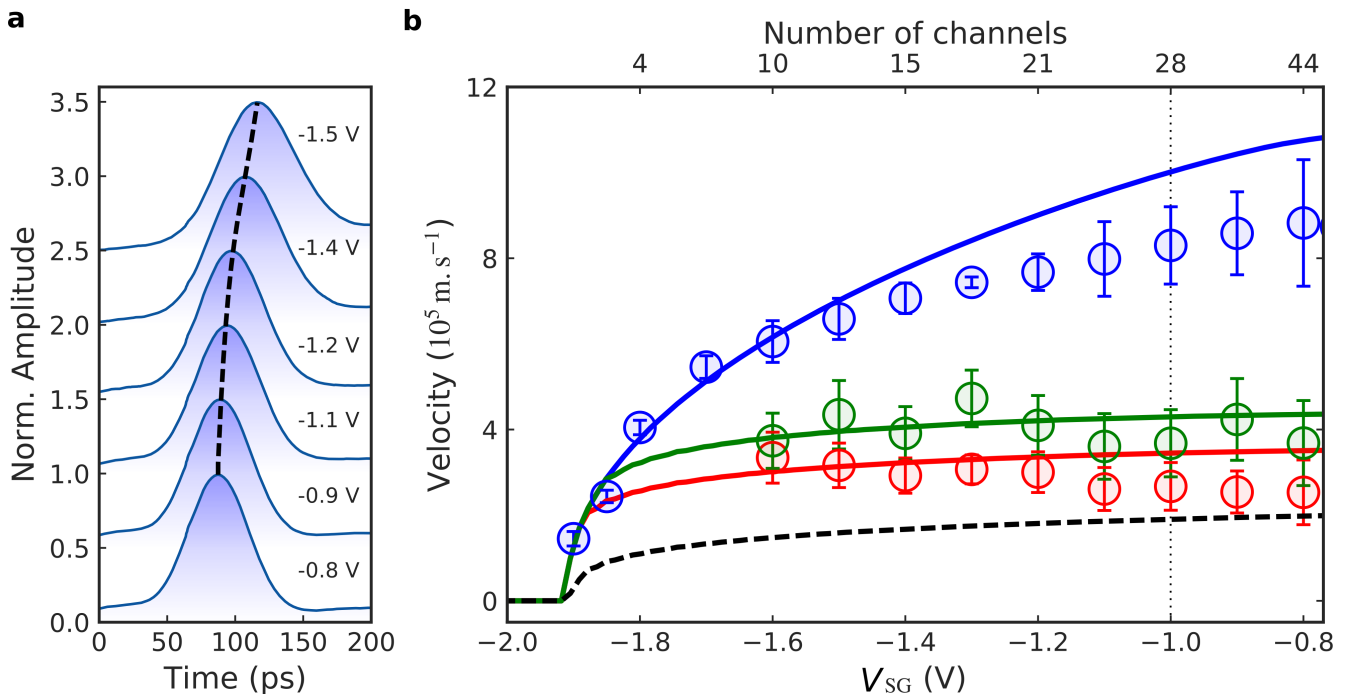


FIG. 2: **Tuning the propagation velocity.** **a**, Time-resolved measurements of the electron pulse for different confinement potentials. The curves have been offset vertically for clarity. **b**, Velocity of the electron pulse as a function of the confinement potential and the corresponding number of channels. open circles: experimental data, solid lines: parameter free self-consistent calculation. The blue data points correspond to situation where the channel filtering QPC<sub>0</sub> is not activated. The red (green) data are obtained by setting the channel filtering QPC<sub>0</sub> at a conductance value of  $G = 2e^2/h$  ( $G = 4e^2/h$ ). The red (green) solid line is a calculation where only the lowest (two lowest) channels are populated. The black dashed line corresponds to non-interacting Fermi liquid. The vertical dotted line indicates the gate voltage at which the velocities of Fig. 3d are taken.

[22].

When we gradually reduce the number of channels to one we enter the Tomonaga-Luttinger liquid regime [1]. However, due to the strong confinement potential and its long length, the quantum wire is not very homogeneous and the pulse becomes distorted. It is therefore not possible to realise a clean one-channel Tomonaga-Luttinger liquid [23] in the present configuration. To circumvent this limitation we have placed another QPC<sub>0</sub> at the entrance of the quantum wire in order to filter specific modes schematised in Fig. 3c. We set the confinement potential of the quantum wire to a situation where the wire width is relatively large ( $V_{SG} = -1.0V$ ;  $N_{modes} \approx 28$ ) and set the quantum point conductance to a value of  $G_{QPC_0} = 2e^2/h$ . First, an electron pulse populating initially 28 modes of the quantum wire passes through the QPC<sub>0</sub> and during the passage only the lowest mode of the quantum wire is transmitted as shown in Fig. 3c. After the passage, the electron pulse continues propagation along the quasi one-dimensional wire containing again the same number of available modes as before the passage through the mode filtering QPC<sub>0</sub>. Assuming a non-adiabatic passage, the wave packet should rapidly fractionalise into a fast plasmon mode and N-1 slow charge modes upon propagation. Very surpris-

ingly, this is not the case. Time-resolved measurements of the electron wave packet passage at QPC<sub>1</sub>, QPC<sub>2</sub> and QPC<sub>3</sub> allow us to determine the average speed of the wave packet after mode selection. We observe that the wave packet is strongly slowed down after passing the mode selection QPC<sub>0</sub> as shown in Fig. 3b and d. These measurements are repeated for different confinement potentials to corroborate our findings (see red data points in Fig.2b). From our theoretical model we can calculate the speed of the electron wave packet assuming that only *one single mode* is occupied after passing the mode selection QPC<sub>0</sub> and compare it to our experimental value as shown by the solid red curve. The agreement between theory and experiment is again remarkable. We have repeated the experiments for the second quantised plateau (green data points) and find similar agreement. It is therefore possible to form a very clean 1 channel (2 channel) Tomonaga-Luttinger liquid where the electron pulse populates only the lowest mode (lowest two modes) of the quantum wire while propagating over a distance of more than 20 micrometers. This is in stark contrast to experiments in the quantum Hall regime, where the wave packet fractionalises already after a distance of less than  $3 \mu m$  [13]. Only at a distance of about 70 micrometers (QPC<sub>3</sub>), we observe that the velocity is again approach-

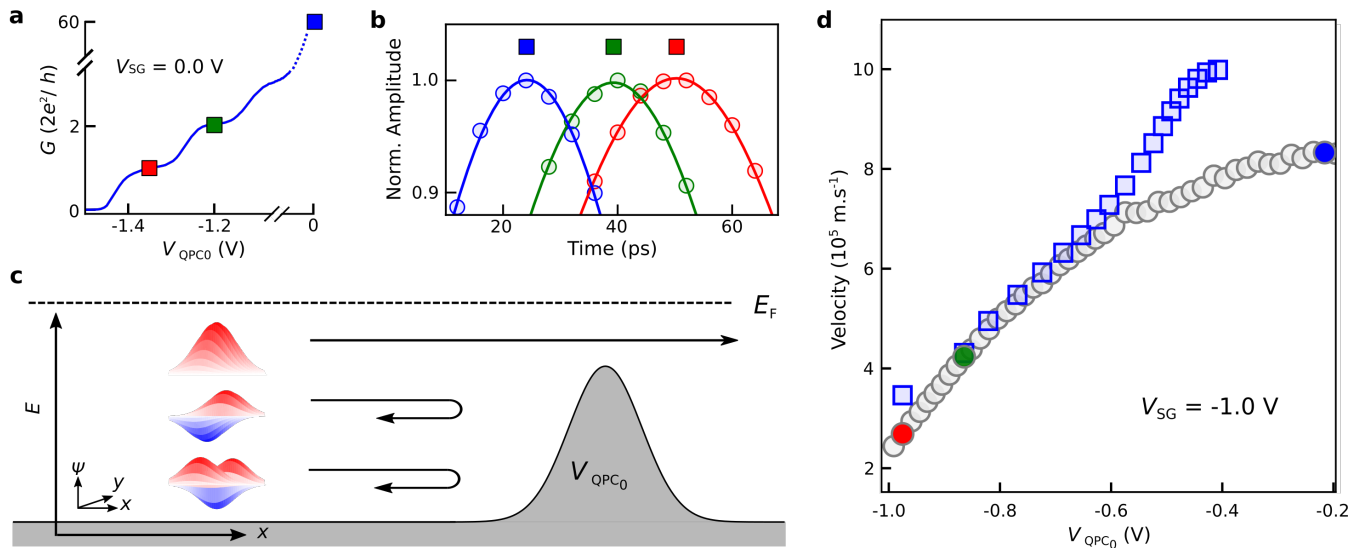


FIG. 3: **Mode selection of an electron pulse.** **a**, Conductance trace of the mode filtering QPC<sub>0</sub> for  $V_{SG} = 0.0$  V. **b**, Time-resolved measurements of the electron pulse propagation at QPC<sub>1</sub> position, when QPC<sub>0</sub> is deactivated (blue), or set to a conductance of  $G = 2e^2/h$  (red) and  $G = 4e^2/h$  (green). **c**, Schematic of the mode filtering experiment. The propagating voltage pulse populates all the available modes of the quantum wire (here for illustration purposes we show 3) before passing through the mode filtering QPC<sub>0</sub>. The mode filtering, which is set to  $G = 2e^2/h$  reflects all modes except the one with the highest kinetic energy. After passing the mode filtering QPC, only this mode is populated and all the others are unoccupied. **d**, Propagation velocity of the electron pulse as a function of the mode selection QPC<sub>0</sub> voltage at a fixed confinement potential  $V_{SG} = -1.0$  V. The grey circles correspond to the experimentally measured velocity at QPC<sub>1</sub> while the blue squares is the outcome of a parameter-free calculation (see suppl. mat.). The coloured circles correspond to the velocity measured for different conductance values of QPC<sub>0</sub>, i.e.  $G = 2e^2/h$  (red circle),  $G = 4e^2/h$  (green circle) and fully depolarised QPC<sub>0</sub> (blue circle). These data points correspond to the dotted vertical line in Fig. 2b at  $V_{SG} = -1.0$  V.

ing the one corresponding to the fast mode where all the modes of the quantum wire are populated. This opens the possibility to realise flying qubit experiments [24, 25] with single electron pulses by only populating a single mode, which has never been observed with DC measurements.

Our findings give also a new insight into the recently discovered Levitons [4]. As the underlying physics is independent of the actual shape of the single electron wave packet, Levitons should be regarded as a special kind of plasmon with the particularity that it does only generate electronic excitations (no holes), rather than a single electron excitation propagating at the surface of the Fermi sea with the Fermi velocity [26].

The presented time control of single electron pulses at the picosecond level will be important for studying real time dynamics of a quantum nano-electronic device [27] and will open the possibility to measure the time spreading as well as the charge fractionalisation dynamics of the electron wave packet during propagation.

## Methods

### Sample fabrication

The sample is fabricated by depositing electrostatic gates

on top of a GaAs/AlGaAs semiconductor heterostructure. The two-dimensional electron gas, which is at a depth of 100 nm, has density  $n = 2.11 \times 10^{11} \text{ cm}^{-2}$  and mobility  $\mu = 1.89 \times 10^6 \text{ cm}^{-2} \text{ V}^{-1} \text{ s}^{-1}$ , measured at 4 K. The 70  $\mu\text{m}$  long electrostatic gates are defined by Ti/Au while a Ni/Ge/Au/Ni/Au alloy is used for the ohmic contacts. A scanning electron microscope image of our sample is shown in figure 4.

### Low temperature measurements

To generate a single electron pulse a voltage pulse with an amplitude of several tens of  $\mu\text{V}$  is applied to the left ohmic contact of our sample through a high bandwidth coaxial line and a 40 dB attenuation. The voltage pulses are provided by an arbitrary function generator (Textronics AWG7122C) and have a 600 MHz repetition frequency. The generated DC current is measured across a 10 k $\Omega$  resistor placed on the sample chip carrier at a temperature of 20 mK. The pulse train is modulated at a frequency of 12 kHz to perform lock-in measurements. A second voltage pulse is applied to one of the QPCs in order to operate it as a fast switch. By changing the time delay between generating the electron pulse and opening/closing the QPC switch we can reconstruct in a time-resolved manner the time trace of the electron pulse, following the protocol developed by Kamata *et al.*

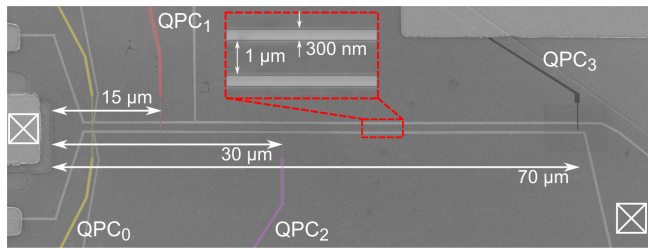


FIG. 4: **Scanning electron microscope image of the nanoelectronic device.** The light grey parts correspond to the electrostatic gates. The long quasi-1D channel has length of  $70 \mu\text{m}$  and width of  $1 \mu\text{m}$ . The two ohmic contacts, one used for the excitation of the electron pulse (left) and the other one used for current detection (right) are indicated with crossed square boxes. The three QPC switches and their respective distance from the left ohmic contact are shown with red, pink and black colors, whereas the mode selection QPC<sub>0</sub> is highlighted with yellow color.

[17].

In order to obtain the shortest possible switching times we perform the following operations, shown in Fig. 5a. First, the QPC is set to the pinch-off regime (OFF - position) by applying an appropriate negative DC voltage ( $V_{\text{DC}}$ ). Subsequently, we apply a short voltage pulse with fixed amplitude ( $V_{\text{AC}}$ ) to the QPC, which allows us to open the QPC switch only on a very short time-scale  $\delta\tau$ , typically below 10 ps [28]. To achieve these fast switching times we keep the  $V_{\text{AC}}$  amplitude constant and we vary  $V_{\text{DC}}$ . As shown in Fig. 5a when  $V_{\text{DC}}$  is very negative the QPC switch remains closed for all time delays and therefore the recorded current is zero. By increasing  $V_{\text{DC}}$  to the appropriate value we can open the QPC switch for a brief period of time  $\delta\tau$ , thus allowing us to reconstruct the electron pulse. As the switching profile of the QPC depends on the combination of the applied DC and AC voltages as well as the very sharp conductance response we can achieve time resolutions that are shorter than those provided by our electronics. By optimising  $V_{\text{DC}}$  and  $V_{\text{AC}}$  amplitudes we were able to measure single electron pulses down to a FWHM of 68ps, as shown in Fig. 5b.

### Time of flight measurements

To determine the velocity of the electron wave packet we performed “time of flight” measurements for different confinement potentials (see Fig. 1 and Fig. 2). For every confinement potential we carry out three independent measurements, one for each QPC (except QPC<sub>0</sub> which is not connected to a bias tee). During these measurements we excite the electron wave packet and measure the time it takes to propagate to the three detection QPCs. By using the “time of flight” and the exact distance between the left ohmic contact (excitation location) and these three QPCs (Fig. 4) we can calculate the velocity

(see suppl. material).

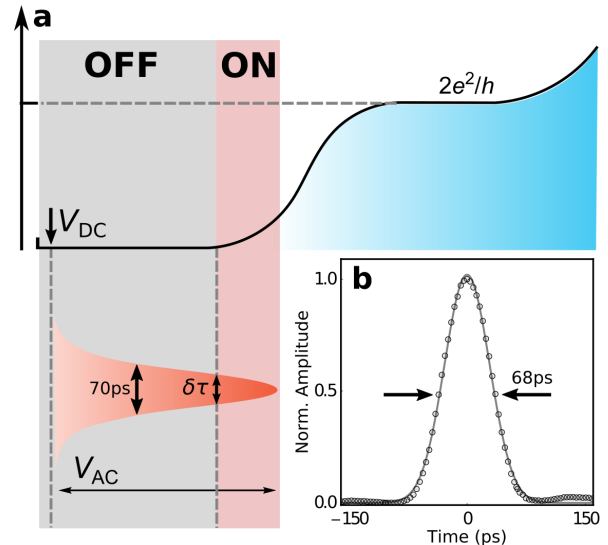


FIG. 5: **A QPC as a fast switch.** **a**, Operation diagram of our fast QPC switch. Initially we apply a negative DC voltage ( $V_{\text{DC}}$ ) on the QPC to set it deep into the pinch-off regime. Then we apply a fast pulse on the QPC,  $V_{\text{AC}}$ , and gradually shift the DC voltage to higher values. By carefully choosing the right  $V_{\text{DC}}$  we can open the QPC for a very short time,  $\sim 10$  ps. **b**, Time resolved measurement of the electron pulse. The dark points are measurements and the continuous line is a gaussian fit. The FWHM of the electron pulse is 68 ps.

### Acknowledgments

Sh. T. acknowledges financial support from the European Union’s Horizon 2020 research and innovation program under the Marie Skłodowska-Curie grant agreement No. 654603. A. L. and A. D. W. acknowledge gratefully support of DFG-TRR160, BMBF - Q.com-H 16KIS0109, and the DFH/UFA CDFA-05-06. C. B, T.M. and X.W. acknowledge financial support from the French National Agency (ANR) in the frame of its program ANR Fully Quantum Project No. ANR-16-CE30-0015-02 and QTERA No. ANR-15-CE24-0007-02. C.B. and T.M. also acknowledge the SingleEIX Project No. ANR-15-CE24-0035. X.W. and P.A. are funded by the U.S. Office of Naval Research.

† These authors contributed equally to this work

**Supplementary information** accompanies this paper.

- 
- [1] Giamarchi, T. *Quantum Physics in One Dimension* (OXFORD UNIV PRESS, 2003).
- [2] Deshpande, V. V., Bockrath, M., Glazman, L. I. & Yacoby, A. Electron liquids and solids in one dimension. *Nature* **464**, 209–216 (2010).
- [3] Fève, G. *et al.* An On-Demand Coherent Single-Electron Source. *Science* **316**, 1169–1172 (2007).
- [4] Dubois, J. *et al.* Minimal-excitation states for electron quantum optics using levitons. *Nature* **502**, 659–663 (2013).
- [5] Auslaender, O. M. *et al.* Spin-Charge Separation and Localization in One Dimension. *Science* **308**, 88–92 (2005).
- [6] Steinberg, H. *et al.* Charge fractionalization in quantum wires. *Nature Physics* **4**, 116–119 (2007).
- [7] Pecker, S. *et al.* Observation and spectroscopy of a two-electron wigner molecule in an ultraclean carbon nanotube. *Nature Physics* **9**, 576–581 (2013).
- [8] Jompol, Y. *et al.* Probing Spin-Charge Separation in a Tomonaga-Luttinger Liquid. *Science* **325**, 597–601 (2009).
- [9] Pham, K.-V., Gabay, M. & Lederer, P. Fractional excitations in the luttinger liquid. *Phys. Rev. B* **61**, 16397–16422 (2000).
- [10] Levkivskiy, I. P. & Sukhorukov, E. V. Dephasing in the electronic mach-zehnder interferometer at filling factor  $\nu = 2$ . *Phys. Rev. B* **78**, 045322 (2008).
- [11] Inoue, H. *et al.* Charge fractionalization in the integer quantum hall effect. *Physical Review Letters* **112** (2014).
- [12] Kamata, H., Kumada, N., Hashisaka, M., Muraki, K. & Fujisawa, T. Fractionalized wave packets from an artificial Tomonaga-Luttinger liquid. *Nature Nanotechnology* **9**, 177–181 (2014).
- [13] Freulon, V. *et al.* Hong-Ou-Mandel experiment for temporal investigation of single-electron fractionalization. *Nature Communications* **6**, 6854 (2015).
- [14] Hashisaka, M., Hiyama, N., Akiho, T., Muraki, K. & Fujisawa, T. Waveform measurement of charge- and spin-density wavepackets in a chiral tomonaga-luttinger liquid. *Nature Physics* **13**, 559–562 (2017).
- [15] Ashoori, R. C., Stormer, H. L., Pfeiffer, L. N., Baldwin, K. W. & West, K. Edge magnetoplasmons in the time domain. *Phys. Rev. B* **45**, 3894–3897 (1992).
- [16] Ernst, G., Haug, R.J., Kuhl, J., von Klitzing, K., Eberl, K. Acoustic Edge Modes of the Degenerate Two-Dimensional Electron Gas Studied by Time-Resolved Magnetotransport Measurements, *Phy. Rev. Lett.* **77**, 4245 (1996).
- [17] Kamata, H., Ota, T., Muraki, K. & Fujisawa, T. Voltage-controlled group velocity of edge magnetoplasmon in the quantum Hall regime. *Phys. Rev. B* **81**, 085329 (2010).
- [18] Kataoka, M. *et al.* Time-of-flight measurements of single-electron wave packets in quantum hall edge states. *Phy. Rev. Lett.* **116** 126803 (2016).
- [19] Kumada, N. *et al.* Plasmon transport in graphene investigated by time-resolved electrical measurements. *Nature communications* **4**, 1363 (2013).
- [20] van Houten, H. *et al.* Coherent electron focussing in a two-dimensional electron gas. *Europhys. Lett.* **5**, 721 (1988).
- [21] Chaplik, A. Absorption and emission of electromagnetic waves by two-dimensional plasmons. *Surface Science Reports* **5**, 289–335 (1985).
- [22] Matveev, K. & Glazman, L. Coulomb blockade of tunneling into a quasi-one-dimensional wire. *Phy. Rev. Lett.* **70**, 990–993 (1993) and Conductance and Coulomb blockade in a multi-mode quantum wire. *Physica B* **189**, 266–274 (1993).
- [23] Jezouin, S. *et al.* Tomonaga-Luttinger physics in electronic quantum circuits. *Nature Communications* **4**, 1802 (2013).
- [24] Yamamoto, M. *et al.* Electrical control of a solid-state flying qubit. *Nature Nanotechnology* **7**, 247–251 (2012).
- [25] Bautze, T. *et al.* Theoretical, numerical, and experimental study of a flying qubit electronic interferometer. *Phys. Rev. B* **89**, 125432 (2014).
- [26] Levitov, L. S., Lee, H. & Lesovik, G. B. Electron counting statistics and coherent states of electric current. *J. Math. Phys.* **37**, 4845–4866 (1996).
- [27] Gaury, B. & Waintal, X. Dynamical control of interference using voltage pulses in the quantum regime. *Nature Communications* **5**, 1–11 (2014).
- [28] Johnson, N. *et al.* Ultrafast Voltage Sampling using Single-Electron Wavepackets. *Applied Phys. Lett.* **110**, 102105 (2017).

# Supplementary Information: Unveiling the bosons in an ultra-short single electron pulse

Gregoire Roussely<sup>†,1</sup> Everton Arrighi<sup>†,1</sup> Giorgos Georgiou,<sup>1,2</sup> Shintaro Takada,<sup>1,3</sup> Martin Schalk,<sup>1</sup> Matias Urdampilleta,<sup>1</sup> Arne Ludwig,<sup>4</sup> Andreas D. Wieck,<sup>4</sup> Pacome Armagnat,<sup>5</sup> Thomas Kloss,<sup>5</sup> Xavier Waintal,<sup>5</sup> Tristan Meunier,<sup>1</sup> and Christopher Bäuerle<sup>1</sup>

<sup>1</sup>*Univ. Grenoble Alpes, CNRS, Grenoble INP,*

*Institut Néel, 38000 Grenoble, France*

<sup>2</sup>*Univ. Savoie Mont-Blanc, CNRS,*

*IMEP-LAHC, 73370 Le Bourget du Lac, France*

<sup>3</sup>*National Institute of Advanced Industrial Science and Technology (AIST),*

*National Metrology Institute of Japan (NMIJ), Tsukuba, Ibaraki 305-8563, Japan*

<sup>4</sup>*Lehrstuhl für Angewandte Festkörperphysik, Ruhr-Universität Bochum,*

*Universitätsstrasse 150, 44780 Bochum, Germany.*

<sup>5</sup>*Univ. Grenoble Alpes, CEA, INAC-Pheligs, 38000 Grenoble, France*

## NUMBER OF INJECTED CHARGES

The number of electrons injected into the quasi-1D channel can be arbitrarily tuned by the voltage applied on the left ohmic contact,  $V_p$ , [1]

$$n_e = 2 \frac{e}{h} \int V_p(t) dt,$$

where  $n_e$  is the number of excited electrons,  $h$  is Plank's constant and  $e$  is the elementary charge. In this formula we assume a single channel of conductance as well as spin degeneracy. The voltage on the left ohmic contact,  $V_p(t)$ , can be calculated directly from the voltage amplitude applied by the AWG on the RF line and by taking into account the appropriate line attenuation.

To estimate the number of generated electrons contained in one electron pulse we measure the rectified current across a 10 k $\Omega$  resistor, which is amplified and measured with a lock-in amplifier. The measured signal is then proportional to the number of generated electrons  $\tilde{n}_e$  distributed over all available conduction channels and to the repetition rate of our AWG, which is  $f = 600$  MHz, i.e.,

$$I = \tilde{n}_e e f = \frac{V_{\text{rms}}}{g} \frac{1}{10 \text{ k}\Omega} \frac{\pi}{\sqrt{2}}$$

where  $V_{\text{rms}}$  is the voltage measured with the lock-in amplifier,  $g = 1000$  is the amplifier gain and the constant factor  $\pi/\sqrt{2}$  is to account for the 12 kHz square pulse modulation signal used for the lock-in detection. As shown in Fig. 1d of the manuscript we can excite from 0.6 to 6.1 electrons per pulse by varying the amplitude of the input pulse.

## TIME CALIBRATION OF RF LINES

The RF lines used for the excitation and detection of the electron pulse are calibrated using two methods, reflectometry measurements and in-situ calibration.

To perform the reflectometry calibration we initially send a short pulse through the RF line and measure the reflected pulse with a high bandwidth oscilloscope. As shown in Fig. S1 we can estimate the relative time delay between the four RF lines by looking at the reflected pulses. This approach offers limited time accuracy ( $\approx \pm 5$  ps) since the RF lines cannot be calibrated with the attenuators installed. A second and more precise calibration can be done in-situ by exploiting the fast propagation of the 2D plasmon.

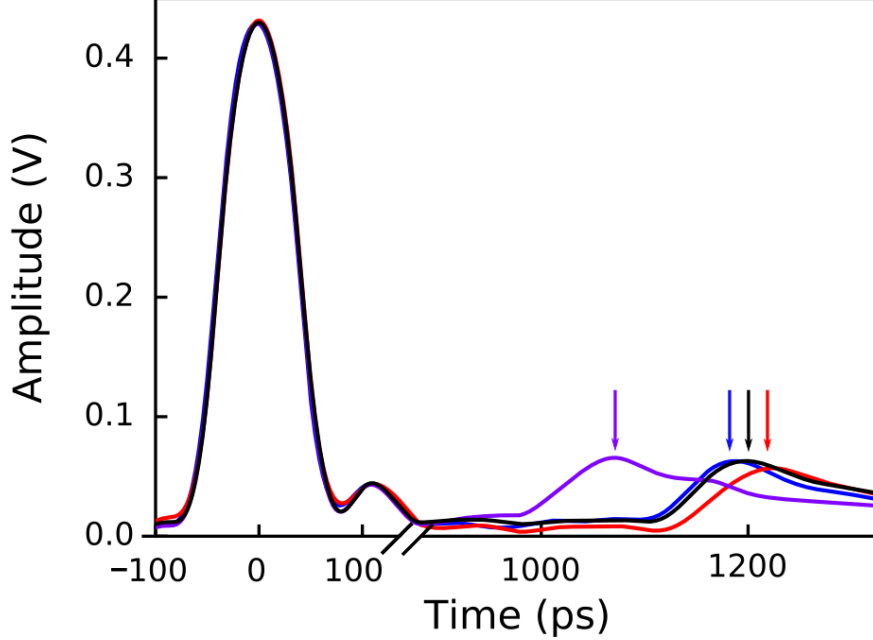


FIG. S1: **Time domain reflectometry**. The large amplitude curves at 0 ps are the pulses applied on the RF lines, while the smaller amplitude curves above 1000 ps are the reflected pulses. The four arrows indicate the peak of the reflected pulse connected to the ohmic contact (blue curve), QPC<sub>1</sub> (red curve), QPC<sub>2</sub> (purple curve), QPC<sub>3</sub> (black curve).

To do so, we almost completely depolarise the 1D channel gates. The collective motion of electrons in this almost confinement-free system has the velocity of a 2D plasmon, which is well known to be  $v_{\text{plasmon}}^{2D} \sim 10^7 \text{ m s}^{-1}$  [2, 3]. When the 2D plasmon is injected at the left ohmic contact it will reach the sampling QPC essentially instantaneously. By measuring a time resolved trace of the 2D plasmon pulse we can estimate the relative time delay between the excitation RF line and the detection QPC RF lines. This allows us to calibrate our RF lines with an accuracy in the order of  $\pm 2$  ps.

### TIME OF FLIGHT MEASUREMENTS – VELOCITY CALCULATION

The velocities shown in Fig. 2b of the manuscript (blue data points) are derived from “time-of-flight” measurements. As it was briefly explained in the methods section, to determine the velocities we performed three independent measurements, one for each QPC (except QPC<sub>0</sub> which is not connected to a bias tee). For each measurement we monitored the “time-of-flight” of the electron wavepacket from the left ohmic contact to the respective QPC,

resulting into  $t_1$ ,  $t_2$  and  $t_3$  for QPC<sub>1</sub>, QPC<sub>2</sub> and QPC<sub>3</sub> respectively. The distance of the three QPCs from the left ohmic contact are derived from the Scanning Electron Microscope (SEM) image of our sample, shown in Fig. 4, and they are  $d_1 = 15 \mu\text{m}$ ,  $d_2 = 30 \mu\text{m}$  and  $d_3 = 70 \mu\text{m}$ .

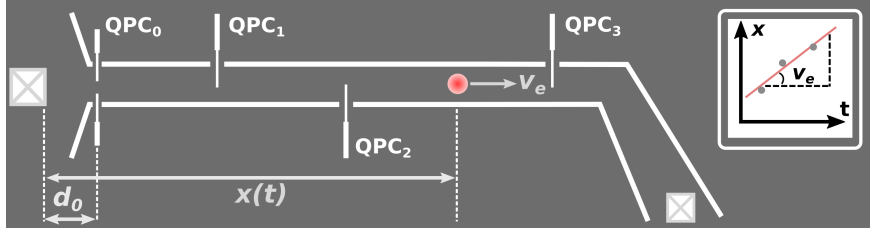


FIG. S2: **Velocity calculation.** Schematic illustrating the velocity calculation from the time-of-flight measurements. The electron wave packet (red sphere) is excited at the left ohmic contact (white crossed square) and it travels a distance  $d_0$  before passing through the mode selection QPC<sub>0</sub> and entering the quasi-1D wire. The wave packet will then travel at a speed  $v_e$  towards the three detection QPCs where a time-of-flight measurement is performed. The inset shows how the speed is derived from the three independent measurements.

As illustrated by Fig. S2, the electron wave packet excited at the left ohmic contact will cover a distance  $d_0$  with speed  $u_0$  before it reaches the mode selection QPC<sub>0</sub>. After passing through the mode selection QPC<sub>0</sub>, the electron wave packet will enter into the quasi-1D channel and travel towards the three QPCs with speed  $v_e$ . The equation governing the motion of the electron has the following form,

$$\begin{aligned} x &= v_0 t_0 + v_e(t - t_0) \\ &= d_0 + v_e t \end{aligned}$$

where  $x$  is the distance from the left ohmic contact to the three QPCs and  $t$  is the “time-of-flight”. The speed can be calculated from the slope of the above equation through a linear fit, as indicated by the inset of Fig. S2.

## SIMULATING THE PLASMON DISPERSION RELATION FROM THE MICROSCOPIC MODEL

A sketch of the system used in our simulations is shown in Figure 1c of the main text. We consider a 3D system with translational invariance along the x direction and with the 2D electron gas situated at  $z = 0$ . The two top gates, situated at  $z = 100$  nm are used for defining the quasi-one dimensional wire, but also provide screening to the electron gas.

Our starting point is a many-body Hamiltonian that describes our 2D electron gas,

$$H = -\frac{\hbar^2}{2m^*} \sum_{\sigma} \int d^2\vec{r} c_{\vec{r}\sigma}^{\dagger} \Delta c_{\vec{r}\sigma} + \sum_{\sigma} \int d^2\vec{r} U(\vec{r}) c_{\vec{r}\sigma}^{\dagger} c_{\vec{r}\sigma} + \sum_{\sigma\sigma'} \int d^2\vec{r} d^2\vec{r}' c_{\vec{r}\sigma}^{\dagger} c_{\vec{r}\sigma} G(\vec{r}, \vec{r}') c_{\vec{r}'\sigma'}^{\dagger} c_{\vec{r}'\sigma'} \quad (1)$$

where the fermionic operator  $c_{\vec{r}\sigma}^{\dagger}$  ( $c_{\vec{r}\sigma}$ ) creates (destroys) an electron at position  $\vec{r} = (x, y)$  and with spin  $\sigma$ ,  $m^*$  is the effective mass,  $\Delta$  the 2D Laplacian operator,  $U(\vec{r})$  an electrostatic potential and  $G(\vec{r}, \vec{r}')$  the electron-electron interaction. In free space,  $G(\vec{r}, \vec{r}')$  is simply given by the bare Coulomb repulsion  $G(\vec{r}, \vec{r}') = \frac{e^2}{4\pi\epsilon|\vec{r}-\vec{r}'|}$ . However, here, the presence of the electrostatic gates provides some screening, and  $G(\vec{r}, \vec{r}')$  is the solution of the 3D Poisson equation (restricted to the 2D gas),

$$\Delta_{3D}G(\hat{r}, \hat{r}') = -\frac{e^2}{\epsilon}\delta(\hat{r} - \hat{r}') \quad (2)$$

with the boundary condition  $G(\hat{r}, \hat{r}') = 0$  when the 3D vector  $\hat{r} = (x, y, z)$  coincides with the position of a gate.  $e > 0$  is the electron charge and  $\epsilon$  the dielectric constant.

### Self-consistent electrostatic-quantum problem

The first step in our calculation is a mean field (self-consistent Hartree) treatment of Eq.(1), in which we aim at solving together the following equations,

$$\Delta_{3D}U(\hat{r}) = -\frac{e\rho(\hat{r})}{\epsilon} + \frac{e\rho_0(\hat{r})}{\epsilon} \quad (3a)$$

$$\frac{-\hbar^2}{2m^*}\Delta\Psi(\vec{r}) - eU(\vec{r})\Psi(\vec{r}) = E\Psi(\vec{r}) \quad (3b)$$

$$\rho(\vec{r}) = \sum_E f(E)|\Psi(E, \vec{r})|^2 \quad (3c)$$

where  $U(\vec{r})$  is the restriction of  $U(\hat{r})$  to the 2D plane of the electron gas,  $\rho(\hat{r}) = \rho(\vec{r})\delta(z)$ ,  $\Psi$  the electronic wave function,  $f$  the Fermi function and the continuum sum in Eq.(3c)

spans over all the eigenstates of the Schrödinger equation (3b). The density  $\rho_0$  accounts for the layer of dopants present above the 2D gas; we use  $U(\hat{r}) = V_{\text{SG}}$  in the top gate and Von Neumann boundary conditions otherwise. We have explicitly verified that the finite width of the 2D gas along  $z$  does not play a role in these calculations. Translational invariance along  $x$  implies that the Poisson equation can be solved in the 2D  $(y,z)$  plane while the wave-function is a plane wave, which can be separated into a transverse and a longitudinal component  $\Psi(E, \vec{r}) = e^{ik_\alpha(E)x}\psi_\alpha(y)$ . Performing an explicit integration along the longitudinal direction at zero temperature, we arrive at,

$$\Delta U(y, z) = -\frac{e\rho(y)}{\epsilon}\delta(z) + \frac{e\rho_0(y, z)}{\epsilon} \quad (4a)$$

$$-\frac{\hbar^2}{2m^*}\frac{\partial^2}{\partial y^2}\psi_\alpha(y) - eU(y, 0)\psi_\alpha(y) = E_\alpha\psi_\alpha(y) \quad (4b)$$

$$\rho(y) = \frac{2}{\pi}\sqrt{\frac{2m^*}{\hbar^2}}\sum_\alpha|\psi_\alpha(y)|^2\sqrt{E_F - E_\alpha} \quad (4c)$$

where we have introduced the Fermi energy  $E_F$ . The factor 2 accounts for spin degeneracy. The Poisson equation for the potential  $U(y, z)$  is solved on the  $(y, z)$  plane by using finite elements in a rectangular box with Von Neumann boundary conditions on the sides and fixed Dirichlet boundary conditions for the side-gate voltage  $V_{\text{SG}}$ . The size of the box has been chosen such that the results are free from finite size effects. An example of calculation of the Green's function  $G(y, y') \equiv G(y, z = 0; y', z' = 0)$  is shown in Fig. S3 for illustration. The Schrödinger equation is discretized using a simple finite difference scheme and solved using the Kwant package [4]. Solving the sequence of equations (4a), (4b) and (4c) for an input density  $\rho$  results to a new density  $\rho^{\text{out}}$ . The self consistency is reached when  $\rho = \rho^{\text{out}}$  (see Fig. S5 for an example of convergence of our iterative procedure). The self-consistent solutions are obtained using a Newton-Raphson scheme [5]. We use the following parameters: effective mass  $m^* = 0.067m_e$ , dielectric constant  $\epsilon = 12\epsilon_0$  and a fixed dopant density of  $n_d = 3.16 \cdot 10^{11} \text{ cm}^{-2}$ . Note that this density is higher than the bulk 2D density of the gas. We have checked that our results are in fact independent of this value since the actual electronic density is controlled by  $V_{\text{SG}}$ . However, using a lower dopant density prevents us from exploring the high density regime ( $V_{\text{SG}} > -1V$ ) where the quasi-1D wire is not defined anymore. Figure S4 shows a color map of the electronic density as a function of the transverse direction of the wire  $y$  and  $V_{\text{SG}}$ . The critical values of the gate voltage where the wire forms ( $V_{\text{SG}} \sim -0.8V$ , the gas is depleted beneath the gates) and the pinch-off

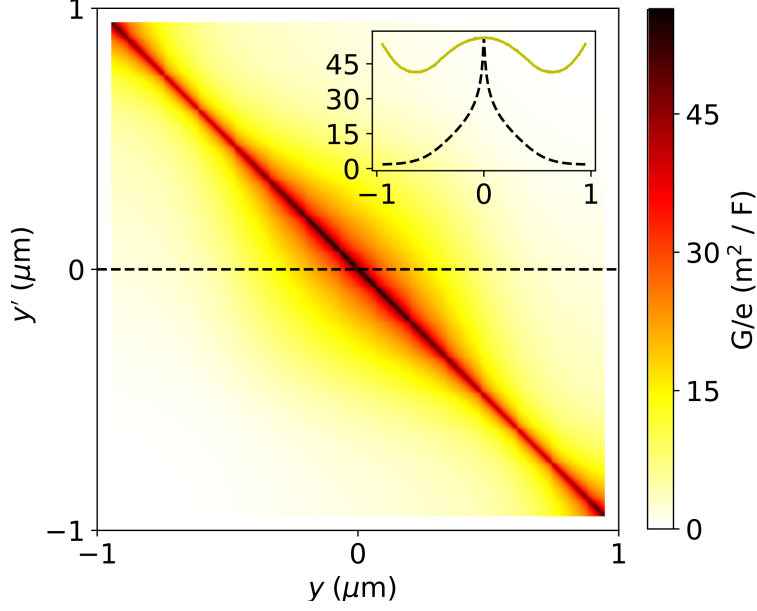


FIG. S3: The Green's function  $G(y, y')$  of the Poisson equation calculated with the finite element method. The two thin regions in the diagonal of the figure at  $y, y' = \pm 0.5$  coincide with the positions underneath the electrostatic gate. In the inset, the black dashed line represents a horizontal cut  $G(y, y' = 0)$  while the solid yellow line is the diagonal part of the matrix  $G(y, y)$ .

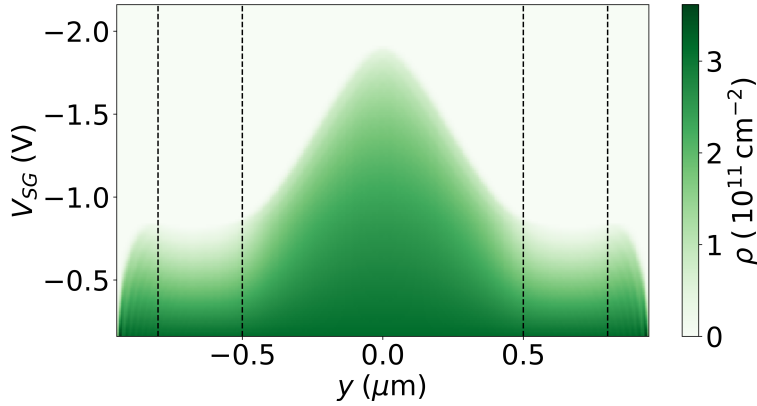


FIG. S4: Colormap: density as a function of the transverse direction of the wire  $y$  ( $\mu\text{m}$ ) and external gate voltage  $V_{SG}$  (V). The vertical black dashed lines show the positions of the two top gates.

( $V_{SG} \sim -1.8\text{V}$ , full depletion) can be clearly identified.

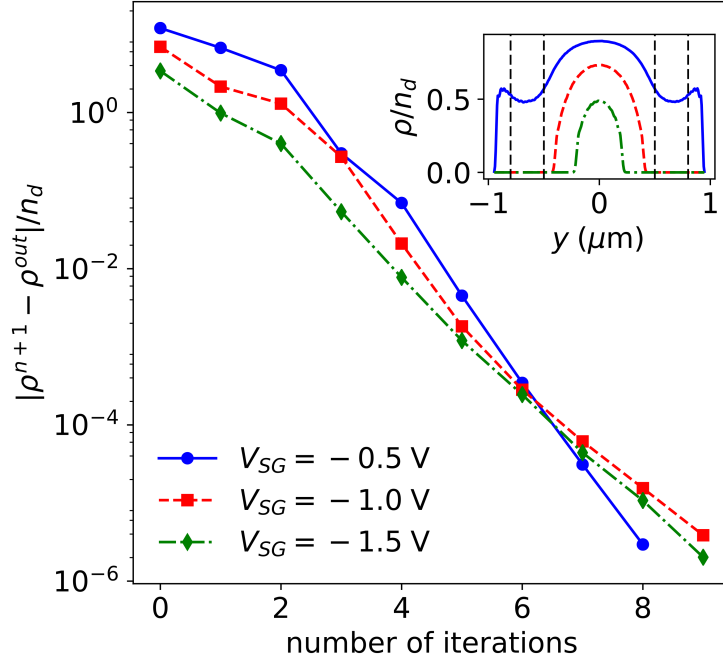


FIG. S5: Convergence of the self-consistent algorithm for three different gate voltages (solid blue: -0.5 V, dashed red: -1.0 V and dash-dotted green: -1.5 V). At each iteration  $n$  we calculate from an input density  $\rho^n$  a new density  $\rho^{n+1}$ . Solving sequentially equation (4) we obtain  $\rho^{out}$  from which we can calculate the distance to the convergence and express it in terms of the dopant density  $n_d = 3.16 \cdot 10^{11} \text{ cm}^{-2}$ . The inset is the converged density for the 3 gate voltages in the same units.

### Generalized Luttinger theory

To proceed, we follow Matveev and Glazman [6] (see also a simpler construction [7]) and construct the bosonised theory for the plasmon excitations of the quasi-1D wire. Bosonization theory predicts that the plasmons have a linear dispersion relation  $\omega = v_P q$ , where  $\omega$  is the plasmon energy,  $v_P$  the plasmon velocity and  $q$  the plasmon wave vector. The values of  $v_P$  are obtained from an eigenvalue problem described below.

In the presence of  $N$  propagating channels, we introduce the  $N \times N$  diagonal velocity matrix  $\tilde{V}$

$$\tilde{V}_{\alpha\beta} = \delta_{\alpha\beta} v_\alpha \quad (5)$$

where  $v_\alpha$  is the non-interacting velocity of mode  $\alpha$ . We also introduce the interaction matrix  $\tilde{G}$  defined as,

$$\tilde{G}_{\alpha\beta} = \sqrt{v_\alpha v_\beta} \int dy dy' |\psi_\alpha(y)|^2 G(y, y') |\psi_\beta(y')|^2 \quad (6)$$

Figure S6 and S7a show examples of the different components of  $\tilde{V}$  and  $\tilde{G}$  for different values of the gate voltage. Once these objects have been defined, the plasmon velocities  $v_P$  can be obtained in a straightforward manner by diagonalising the following matrix,

$$\left( \tilde{V}^2 + \frac{2}{h} \tilde{G} \right) \tilde{n} = v_P^2 \tilde{n} \quad (7)$$

where  $\tilde{n}$  is a  $N$ -sized vector. Typically Eq.(7) has one large eigenvalue and  $N - 1$  small ones due to the low effective rank of the  $\tilde{G}$  matrix (see Fig. S6). The plasmon velocity  $v_P$  is the chief outcome of this calculation and is shown in Fig. S7b.

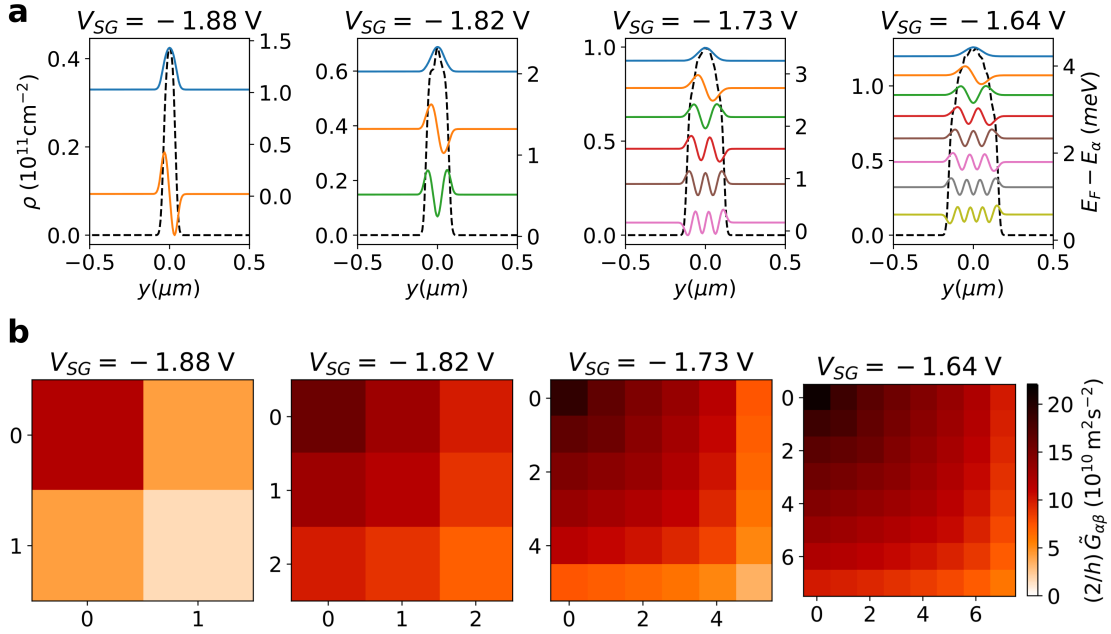


FIG. S6: **a**, Density and wave functions for four different channel gate voltages ( $-1.88$ ,  $-1.82$ ,  $-1.73$  and  $-1.64 \text{ V}$ ). In each plot the black dashed curve represents the self-consistent density  $\rho$  in  $\text{cm}^{-2}$  (left y axis). Each coloured line sketches the shape of the wave function (in arbitrary units) of one open mode  $\psi_\alpha$ , centred around its kinetic energy  $E_F - E_\alpha$  (right y axis). **b**, Green function matrix  $\tilde{G}$  from which we calculate the renormalized velocities, Eq. (7).

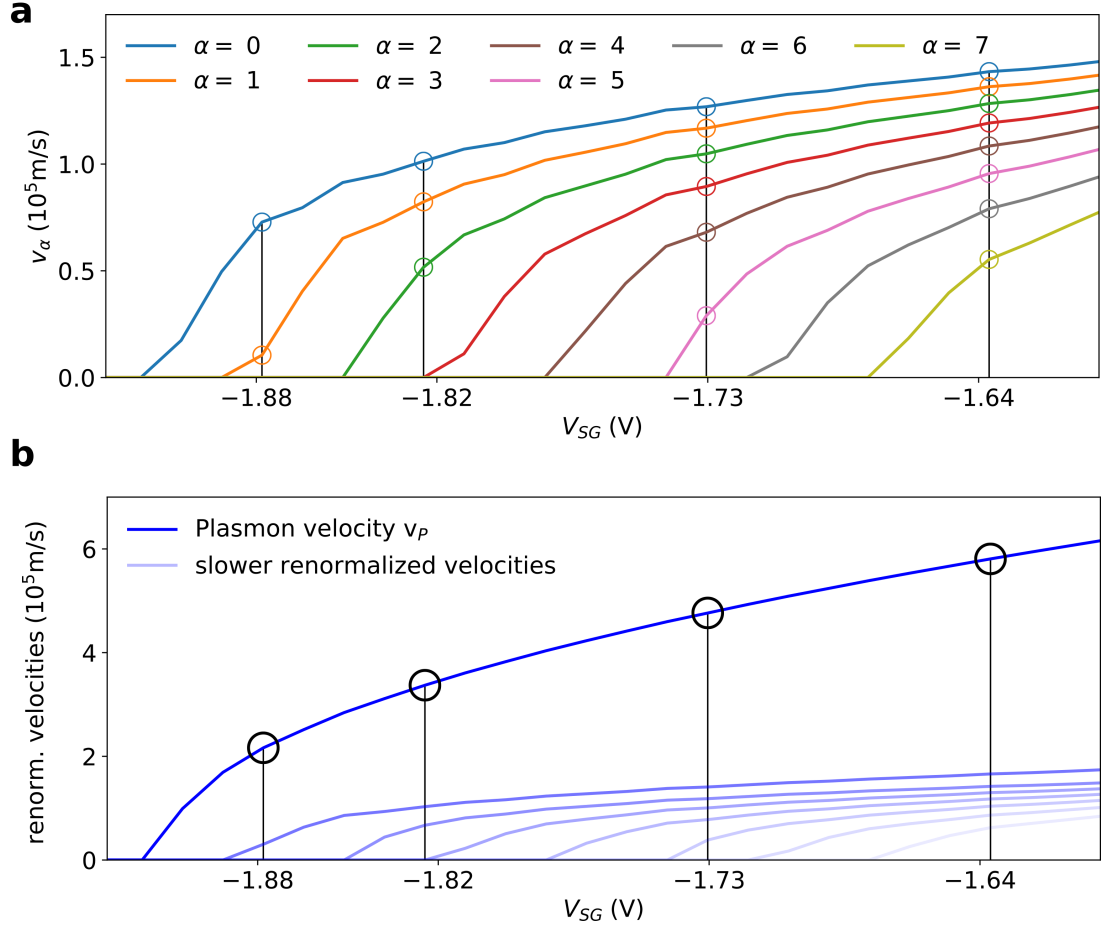


FIG. S7: **a**, Non-interacting velocities  $v_\alpha$  for the open modes as a function of gate voltage  $V_{SG}$ . The four gate voltages ( $-1.88$ ,  $-1.82$ ,  $-1.73$  and  $-1.64$  V) are marked with black vertical lines and the velocities of the corresponding open modes are marked with circles. **b**, Renormalized velocities calculated from Eq. 7 for each gate voltage  $V_{SG}$ . One velocity, indicated by the solid blue line, is considerably higher than the others. This fast collective mode, propagating with velocity  $v_p$ , corresponds to the plasmon mode shown in Fig. 2b of the manuscript.

- 
- [1] Gaury, B. & Waintal, X. Dynamical control of interference using voltage pulses in the quantum regime. *Nature Communications* **5**, 1–11 (2014).
- [2] Chaplik, A. Absorption and emission of electromagnetic waves by two-dimensional plasmons. *Surface Science Reports* **5**, 289–335 (1985).
- [3] Wu, J. *et al.* Excitation, detection and electrostatic manipulation of terahertz-frequency range

- plasmons in a two-dimensional electron system. *Scientific Reports* **5**, 15420 (2015).
- [4] Groth, C. W, Wimmer, M., Akhmerov, A. R. & Waintal, X. Kwant: a software package for quantum transport. *New Journal of Physics* **16**, 063065 (2014).
- [5] Ben-Israel, A. A Newton-Raphson method for the solution of systems of equations. *Journal of Mathematical Analysis and Applications* **15**, 243–252 (1966).
- [6] Matveev, K.A. & Glazman, L.I. Conductance and Coulomb blockade in a multi-mode quantum wire. *Physica B: Condensed Matter* **189**, 266–274 (1993).
- [7] Kloss, T., Weston, J. & Waintal, X. Transient conductance between Fermi and Luttinger liquids. *arXiv:1710.00895* (2017).